Jiang *et al. Cancer Nanotechnology* (2025) 16:8
https://doi.org/10.1186/s12645-025-00312-7

Cancer Nanotechnology

RESEARCH **Open Access**

Integration of temperature-sensitive hydrogels loaded with realgar and magnetic particles for lung cancer diagnosis and treatment

Tao Jiang[1,2†], Zhifei Huang[1,2†], Mingdong Reng[1,2†], Yuwei Ma[1,2], Bo Gao[1,2], Shilong Song[1,2], Fei Liu[3], Xiangyu Zhang[6], Jingwen Huang[1*], Zelai He[1,2*], Huijun Zhang[5*], Jing Ma[4*] and Gengming Wang[1,2*]

†Tao Jiang, Zhifei Huang, and Mingdong Reng have contributed equally to this work.

*Correspondence:
byyfyhjw@163.com;
he.ze.lai@163.com;
Zhanghuijunhp@163.com;
majing0709@163.com;
lansefeidian777@163.com

[1] The First Affiliated Hospital of Bengbu Medical University, Bengbu 233004, China
[2] Department of Radiation Oncology, The First Affiliated Hospital of Bengbu Medical University, Bengbu 233004, China
[3] Anhui Province Key Laboratory of Clinical and Preclinical Research in Respiratory Disease, Molecular Diagnosis Center, Department of Pulmonary and Critical Care Medicine, The First Affiliated Hospital of Bengbu Medical University, Bengbu 233004, China
[4] Section of Echocardiography, Department of Cardiology, Xinhua Hospital Affiliated to Shanghai Jiaotong University School of Medicine, Shanghai 200092, China
[5] Department of Cardiothoracic Surgery, Huashan Hospital of Fudan University, Shanghai 200040, China
[6] Department of Pathology, Jining First People's Hospital, Jining Medical University, Jining 272002, Shandong, China

Abstract

Introduction: Lung cancer has a poor prognosis with traditional treatments. Realgar (AS_4S_4), a traditional Chinese medicine, exhibits chemotherapeutic efficacy. However, its low solubility, complex dosage form, and limited therapeutic efficacy hinder its further application in lung cancer.

Methods: In this study, AS_4S_4 was chemically synthesized using hydrochloric acid to disrupt the bonding between AS and NH_2, producing realgar nanoclusters that improved solubility and reduced side effects. Simultaneously, Fe_3O_4 nanoparticles were introduced, and intelligent temperature-sensitive hydrogels were utilized to combine these two performance nanomaterials, developing a local injection nano-diagnosis and treatment unit (AS_4S_4/Fe_3O_4@Gel) that integrates chemotherapy with alternating current magnetic field (ACMF) induction hyperthermia. The morphological characteristics, thermal stability, and controlled release of AS_4S_4/Fe_3O_4@Gel were assessed. After processing the Lewis cells, the CCK-8 method, hemolysis test, EdU method, cell apoptosis test, reactive oxygen species detection, and cellular ultrastructure analysis were used to evaluate the biological effects. Western blot was employed to detect Bcl-2, BAX, GPX4, and HO-1 protein expression in cells. After injecting the gel system into the transplanted tumor, in vivo imaging, near-infrared thermography, and the antitumor effect were studied.

Results: AS_4S_4/Fe_3O_4@Gel, which exhibits fluorescence and magnetic inductive hyperthermia, was successfully developed. The gel system, which has good hemocompatibility, possesses ideal temperature sensitivity. It can transform from liquid to solid within a specific temperature range, and the drug release rate about 80% within 3 h at 42 °C. Cell experiments showed that the combination of AS_4S_4/Fe_3O_4@Gel and ACMF induced the highest levels of apoptosis and ferroptosis. AS_4S_4/Fe_3O_4@Gel in vivo displayed good fluorescence characteristics and a magnetocaloric effect. The combination therapy group significantly decreased the expression levels of Ki-67, CD31, E-cadherin, Bcl-2, and GPX4 proteins, indicating that combination therapy can better exert antitumor effects. At the same time, AS_4S_4/Fe_3O_4@Gel had no damage to normal organs.

Conclusion: The prepared AS_4S_4/Fe_3O_4@Gel in this study can exert synergistic antitumor activity in combination with ACMF under bimodal imaging guidance and represents a potential clinical treatment for lung cancer.

Keywords: Lung cancer, Realgar, Iron oxide, Chemotherapy, Magnetic induction thermotherapy

Introduction

Lung cancer is currently among the malignant tumors with the highest global morbidity and mortality rates, of which non-small cell lung cancer (NSCLC) is the most common form. While NSCLC treatment is based on surgical resection, systemic chemotherapy, and local radiotherapy, they all have certain limitations (Barr et al. 2024; He et al. 2024). Therefore, exploring more therapeutic strategies for lung cancer is urgent. Nanomedicines have attracted attention in lung cancer treatment due to the characteristics of nanoparticles, including surface effects, quantum size effects, small size effects, macroscopic quantum tunneling effects and the ability to prolong drug circulation time in vivo and to deliver drugs to targeted locations for release. Additionally, certain nanomaterials possess special physical, chemical, and optical properties, enabling them to accurately diagnose or treat cancers, thus minimizing undesirable side effects and enhancing treatment efficacy (Shukla et al. 2022).

Previously, cell death has been classified into three types based on cell morphology: apoptosis, autophagy, and necrosis. In 2012, a novel non-apoptotic cell death pattern, dominated by iron-dependent lipid peroxidation damage, was proposed and named "ferroptosis" (iron death). It is caused by the failure of membrane lipid repair enzyme-glutathione peroxidase 4 (GPX4), impaired metabolism of intracellular lipid peroxides, and the accumulation of iron-dependent lipid reactive oxygen species (ROS) in the cell. The cell death can be caused by the accumulation of ROS induced by a large amount of iron. Researches have found that inhibiting ferroptosis is widespread in lung cancer cells. In lung cancer cells, the increased expression of GPX4 inhibited iron death, implying that the occurrence of iron death in tumor cells can be promoted by inhibiting GPX4 expression. Numerous basic studies have demonstrated that the iron death inducer erastin promotes intracellular ROS accumulation and cell death, and a significant increase in exogenous iron enhances the cell death induced by erastin (Gong et al. 2022; Tabnak et al. 2021; Wu et al. 2021). Magnetic iron oxide (Fe_3O_4) nanomaterials can not only induce iron death, but also have good biocompatibility, superparamagnetism, and functionalized surface modification, applicable to magnetic resonance imaging and corresponding multimodal imaging after surface modification by certain physicochemical methods(Fan et al. 2023; Fernández-Acosta et al. 2022; Abaei et al. 2024; Turrina et al. 2023; Mohaghegh et al. 2022; Zhou et al. 2022).

As a traditional Chinese medicine, realgar (AS_4S_4) can inhibit the deoxyribonucleic acid (DNA) synthesis of cancer cells, induce apoptosis of cancer cells, improve body immunity, and play an anticancer role (Ding et al. 2018; Guan et al. 2022; Hollow and Johnstone 2023; Wu et al. 2011; Yang et al. 2021). However, due to the low solubility and low bioavailability of realgar, it is limited in clinical application. Nano-realgar with smaller particle diameters has been paid attention in antitumor effects due to its stronger penetration ability, significantly higher bioavailability, and so enhancing its toxicity to tumor cells while reducing its toxicity to normal cells (Tian et al. 2014; Xi et al. 2022). Simultaneously, realgar has fluorescent properties and can be used for tumor monitoring.

Temperature-sensitive hydrogels can undergo a reversible phase transition in response to ambient temperature changes. They are known as "reverse temperature-sensitive" materials because they are liquid at low temperatures and solidify at high temperatures. By leveraging the phase transition characteristics of "reverse temperature-sensitive" materials, intelligent drug delivery systems that respond to changes in ambient temperature can be synthesized (Fu et al. 2018; Liu et al. 2020; Tan et al. 2023; Wang et al. 2023a). When injected into the body, the temperature-sensitive hydrogel solidifies in situ under the effect of body temperature. It serves as a drug release carrier to inject the desired concentration of drug mixed with the temperature-sensitive hydrogel into the diseased area, and the gel is formed rapidly. This in situ-formed hydrogel can be firmly bonded to the tumor tissues, releasing the encapsulated drug precisely at the diseased site. This effectively controls the range of drug release from the hydrogel and reduces side effects (Wang et al. 2023b; Liu et al. 2019; Xiao et al. 2021; Ma et al. 2024).

To explore additional therapeutic strategies for lung cancer, we utilized an intelligent temperature-sensitive hydrogel as a carrier. We innovatively combined AS4S4 with Fe_3O_4 nanomaterials, while chemotherapy was matched with magnetic induction thermotherapy to successfully construct a nanodiagnostic and therapy unit with the functions of multimodal imaging and multiple treatment methods in one. In our study, we used a high-frequency external magnetic induction hyperthermia device (> 100 kHz), which has targeted heating characteristics and can concentrate heat in the target tissue area. By adjusting the distribution and parameters of the magnetic field, the normal tissue is less affected by heat and the temperature of the diseased tissue is controlled at around 42–45 °C. This temperature range has a good effect on killing tumor cells or relieving inflammation, while avoiding serious damage to the tissue caused by excessive temperature. At present, there is no relevant report on the form of AS_4S_4-hydrogel. We expect to achieve long-term release of drugs through the controlled release effect of temperature-sensitive hydrogel, and together with the iron death effect and thermotherapy, so as to achieve high antitumor efficiency and relative low toxicity to normal tissue. However, the combined effect and mechanism are still unclear, and this study will conduct in-depth research on this topic.

Experimental materials and methods

Materials

Poloxamer 407 (F127), poloxamer 188 (F68), and hydroxypropyl methylcellulose were obtained from Sigma Reagent (Shanghai, China). Lewis lung cancer cells (Lewis) were provided by the Anhui Laierwen Technology Co. Ltd. Balb/c mice were purchased from Cyanogen Bio Ltd. (Hefei, China). Dimethyl sulfoxide and phosphate-buffered saline (PBS) were acquired from Solarbio (Beijing, China). Dulbecco's modified Eagle medium (DMEM) and fetal bovine serum (FBS) were bought from BioInd (Israel). Tryptic digest and penicillin–streptomycin solution were procured from Biosharp (Shanghai, China).

The cell counting Kit-8 (CCK-8) and Annexin V-FITC Apoptosis Detection Kit were supplied by BestBio (Shanghai, China). Furthermore, 5-ethynyl-2’-deoxyuridine (EdU)−488 Cell Proliferation Kit, bicinchoninic acid (BCA) Protein Quantification Detection Kit, ROS Detection Kit, and TUNEL Apoptosis Detection Kit were obtained from Biyuntian Biotechnology (Shanghai, China)**.** Mouse monoclonal antibody glyceraldehyde 3-phosphate dehydrogenase (GAPDH) and rabbit polyclonal antibody B-cell lymphoma 2 (Bcl-2) were purchased from Proteintech (Wuhan, China). Rabbit monoclonal antibody GPX4 and rabbit monoclonal antibody Bax were acquired from Abcam. Mouse monoclonal heme oxygenase 1 (HO-1) antibody was bought from Affinity Biosciences (Jiangsu, China). Matrigel gel was provided by BD. Enhanced chemiluminescence (ECL)**-**plus chemiluminescence kit and polyvinylidene difluoride (PVDF) membrane were obtained from Millipore.

Methods

AS4S4/Fe3O4@Gel preparation

A total of 1.2 g N-isopropylacrylamide, 0.05 g of potassium persulfate, 0.05 g N,N’-methylenebisacrylamide, and 0.02 g cysteine hydrochloride were dissolved in 50-mL beaker. After magnetic stirring for 1 h, 25 μL of crosslinking agent N,N,N’,N’-tetramethylethylenediamine was added. The hydrogel was obtained by fully stirring under nitrogen protection for 0.5 h. The hydrogel obtained after the reaction was placed in a 10-kDa dialysis bag for dialysis for 3 days, and the thermosensitive responsive hydrogel was obtained after freeze-drying. Using the high-temperature pyrolysis method, 0.7 g iron acetylacetone, 25 mL dibenzyl ether, 3 mL oleic acid and 1 mL oleamide were weighed into a three-neck flask, and the following procedures were set under nitrogen protection: After being kept at 220 ℃ for 60 min, the temperature was heated to 290 ℃ within 30 min. After being kept at 290 ℃ for 30 min, the heat source was turned off; the magnetic beads were separated and washed with ethanol three times. Fe_3O_4@OA with a particle size of 20 nm could be synthesized. Dissolve 25 mg Fe_3O_4@OA solution in 100 mL chloroform and 100 mg dimercaptosuccinic acid (DMSA) in 100 mL acetone and mix thoroughly. The mixture is then mechanically stirred at 65 °C for 12 h. Adjust the PH to 9 and dialysis the solution for 3 days to obtain Fe_3O_4@DMSA. AS_4S_4 was synthesized by chemical method. In addition, 200 mg of realgar powder was added to 20 mL of ethanolamine and reacted at 80 ℃ for 3 days. The solution is then centrifuged through the film and set aside. The pH is adjusted to neutral with hydrochloric acid to break the bond between AS and NH_2 under acidic conditions. Nano-realgar clusters were obtained by washing with purified water 3 times. Fe_3O_4@DMSA and AS_4S_4 were mixed with hydrogel to obtain pot-carrying gel.

Material characterization

The morphology of Fe_3O_4@DMSA and AS_4S_4 was characterized by transmission electron microscopy (TEM, Tecnai). The morphology of empty and drug-loaded hydrogels (AS_4S_4/Fe_3O_4@Gel) was analyzed by scanning electron microscopy (SEM), and the contained elements were measured by Thermo Fisher Scientific (XPS).

The relationship between the shear rate and viscosity of hydrogels was analyzed using a rheometer to test the rheological properties of the hydrogels.

To detect changes in the gel state of hydrogels at different temperatures, the phase transition characteristics of hydrogels were investigated using the tube inversion method. The AS_4S_4/Fe_3O_4@Gel was sealed in a 10-mL glass vial and slowly heated from 25 to 42 °C in a water bath to detect the physical state of hydrogels at 25 and 42 °C (Tan et al. 2023).

The molecular structure and optical properties of AS_4S_4, AS_4S_4/@Gel, and AS_4S_4/Fe_3O_4@Gel were examined using a fluorescence spectrometer and ultraviolet (UV)–visible spectrophotometer.

Inductively coupled plasma (ICP) emission spectroscopy was utilized to verify the in vitro release of nanohydrogels AS_4S_4/Fe_3O_4@Gel at different temperatures.

Finally, select healthy and qualified rabbits with a weight of approximately 2.5 kg. Before the experiment, domestic rabbits should be acclimated to the laboratory environment for at least one day, ensuring they adapt to both the feeding conditions and the experimental procedures. Prior to the experiment, each rabbit underwent a pre-examination to confirm normal body temperature. Only rabbits with a body temperature between 38.0 and 39.6 °C, and with temperature fluctuations not exceeding 0.4 °C, were selected for the study. Subsequently, 200μL of AS_4S_4/Fe_3O_4@Gel was carefully administered subcutaneously into each rabbit, with a total of six injection sites. The injection should be performed at a consistent speed to prevent discomfort or pyrogenic reactions due to excessive speed changes. Rectal temperatures of the rabbits were measured every 30 min for 1 to 3 h post-injection. Temperature readings were recorded, and the rabbits were observed for pyrogenic symptoms such as shivering, piloerection, and vomiting.

Cell culture

After removing the Lewis lung cancer cells frozen in liquid nitrogen, they were immediately rewarmed by rapid shaking in a water bath at 37 °C for 1 min. Then, they were added into a 15-mL centrifuge tube containing complete medium (basal medium + 10% FBS and 1% penicillin and streptomycin), centrifuged at 1000 rpm/3 min, and the supernatant medium was aspirated away in an ultra-clean table and mixed with 1 mL complete medium. The supernatant medium was blended with 1 mL of complete medium and dispersed in dishes containing 5 mL of complete medium. They were then placed in a cell culture incubator at 37 °C with 5% CO_2 for incubation and subsequently passaged after the cell density reached 80% (Zhang and He 2023). The complete medium was removed from the dishes, washed twice with sterilized PBS, digested with 1 mL of trypsin, and finally terminated with medium to prepare the cell suspension for use.

In vitro cytotoxicity assay

Lewis cells in the logarithmic growth phase were spread into 96-well plates (density of 5×10^3 cells/well) and incubated at 37 °C, 5% CO_2 incubator for 24 h. When the cell density reached about 80%, medium solutions containing different concentrations (gel and various concentrations (0, 0.05, 0.1, 0.2, 0.4, 0.8, 1.6, 3.2, 6.4, 12.8, 25.6, 51.2, and 102.4 μg/mL) of medium solutions of AS_4S_4@Gel, Fe_3O_4@Gel, and AS_4S_4/ Fe_3O_4@Gel were incubated with the cells for 24 h. The cells were then removed from the medium solution. Subsequently, the medium solution was discarded, and the cells were washed twice with PBS. They were then treated with a CCK-8 working solution (configured based on CCK-8: DMEM medium = 1:9) and incubated in a 37 °C, 5% CO_2 incubator for 1 ~ 2 h. Absorbance was detected at 450 nm using an enzyme meter under light protection. The in vitro cytotoxicity was evaluated by calculating the cell survival and the LD50 (IC50) of AS_4S_4@Gel, Fe_3O_4@Gel, and AS_4S_4/Fe_3O_4@Gel for cells in different groups.

Cell survival (%) = [(OD experimental group—OD blank control group)/(OD negative control group—OD blank control group)] × 100%.

Protein blot analysis

Lewis cells in the logarithmic growth phase were spread into 6-well plates (density of 1×10^5 cells/well) and incubated at 37 °C, 5% CO_2 incubator for 24 h. After the cells were wall-adhered, Lewis tumor cells were treated with a complete medium solution containing the IC_{50} concentration of AS_4S_4@Gel, Fe_3O_4@Gel, and AS_4S_4/Fe_3O_4@Gel for 24 h. For the magnetically induced thermotherapy (ACMF) group, cell lysates were obtained by whole-cell lysis after thermotherapy of cells with a magnetic induction thermotherapy apparatus for 10 min (power of 390 kHz/2.58KA $\times$ M^{-1}).

The protein concentration was determined using a BCA protein quantification kit. The extracts were separated by sodium dodecyl sulfate–polyacrylamide gel electrophoresis and transferred to the PVDF membrane. The membrane was blocked with 5% bovine serum albumin (BSA) (tris-hydrochloric acid buffer + Tween) in TBST for 1 h at 25 °C and then incubated with primary antibody (dilution ratio: GAPDH 1:5000, Bcl-2 1:1000, Bax 1:1000, GPX4 1:1000, and HO-1 1:1000 at 4 °C overnight. The next day, after washing the membrane, it was incubated with the secondary antibody at room temperature for 2 h. After washing the membrane, ECL▪plus kit chemiluminescence was performed, and the signal was detected by the Bio▪Rad imaging instrument.

In vitro apoptosis assay

Detection was performed using imaging flow cytometry and stained with apoptosis reagent dye FITC/PI. Annexin V-FITC labeled early apoptotic cells, while propidium iodide (PI) labeled mid-late apoptotic and necrotic cells. Lewis cells in the logarithmic growth phase were placed in 6-well plates (density 5×10^6/well) for adherence culture for 24 h. The administration group was added with a complete medium solution containing IC_{50} concentration of AS_4S_4@Gel, Fe_3O_4@Gel, and AS_4S_4/Fe_3O_4@Gel for 24 h. The Gel group was treated with the same concentration of gel solution for co-culture for 24 h. For the ACMF group, the cells were thermo-treated with a magnetic induction thermotherapy apparatus for 9 min. The medium was removed, the cells were washed with PBS twice, and they were digested and prepared into cell suspensions. Annexin V-FITC and PI dyes were added, and the cells were incubated for 15 min under low-light conditions. They were then detected by flow-through under low-light conditions (the excitation wavelength Ex was set to 488 nm, the emission wavelength of FITC was 530 nm, and the emission wavelength of PI was 620 nm). Fluorescent probe channels were selected to collect cells, and the apoptotic degree of the cells was evaluated based on the number of cells in the four quadrants (normal cells, early apoptotic cells, late apoptotic cells, and necrotic cells) in the flow cytometric quadrant diagram.

In vitro cell proliferation assay

Notably, 5-ethynyl-2’-deoxyuridine (EdU) can be incorporated into newly synthesized DNA as a substitute for thymidine during DNA synthesis, and its acetylene group can be modified by fluorescently labeled small molecule azide probes. The newly synthesized DNA would be labeled by the corresponding fluorescent probe, and thus, proliferating cells could be detected by measuring the fluorescence intensity of the probe using a fluorescence detection device. Lewis cells in the logarithmic growth phase were inoculated in 6-well plates at a density of 1×10^5 cells/well. The drug administration group was treated with a complete medium solution containing IC_{50} concentration of AS_4S_4@Gel, Fe_3O_4@Gel, and AS_4S_4/Fe_3O_4@Gel for 24 h. For the ACMF group, the cells were treated for 10 min with a magnetically induced hyperthermia device. A total of 500 μL of EdU-488 (10 μM) medium was added to each well and incubated for 2 h at room temperature. Next, the cells were fixed in a PBS solution containing 4% paraformaldehyde for 15 min, washed with PBS containing 3% BSA for 15 min, and then rinsed three times with PBS buffer. After being permeabilized by a PBS solution containing 0.3% Triton X-100, the cells were rinsed three times with PBS and incubated with 1 × click additive solution for 30 min in the dark. After the PBS was rinsed three times, 1 × 4′,6-diamidino-2-phenylindole reaction solution was added for 30 min at room temperature in the dark. Finally, the cells were observed using an inverted fluorescence microscope (Zeiss, Germany).

Measurement of ROS

DCFH-DA can freely pass through the cell membrane, and when it enters the cell, it can be hydrolyzed under the action of non-specific endogenous esterases to generate DCFH and remain in the cell. When ROS are present, non-fluorescent DCFH can be oxidized by ROS to produce fluorescent DCF. The fluorescence intensity of DCF can be measured using flow cytometry to evaluate intracellular ROS levels. Lewis cells in the logarithmic growth phase were inoculated in 6-well plates (1×10^5 cells/well). After apposition, the drug groups IC_{50} concentration of AS4S4@Gel, Fe3O4@Gel, and AS4S4/Fe3O4@Gel were given medium solution to co-incubate with the cells for 24 h. For the ACMF group, the cells were calorimetered with the magnetically induced calorimetry instrument for 10 min, and the medium was removed. The cells were washed three times with PBS and probed with 10 μM/L concentration of DCFH-DA in a serum-free medium (DMEM). The cells were collected after incubation for 30 min at 37 °C, 5% CO2, and fluorescence detection was performed using the FITC channel of a flow cytometer (excitation wavelength Ex was set to 488 nm, and emission wavelength Em was set to 525 nm).

Transmission electron microscopy (TEM) observation of cellular iron death

One of the major features distinguishing iron death from other types of cell death is mitochondrial morphological changes. When cells underwent iron death, mitochondria mainly exhibited smaller than normal mitochondrial volume, increased density, higher potential, reduced or disappeared cristae, and ruptured outer membrane. Lewis cells in the logarithmic growth phase were inoculated in 6-well plates (1×10^5 cells/well). After wall affixation, the drug group IC50 concentration of AS4S4@Gel, Fe3O4@Gel, and AS4S4/Fe3O4@Gel was administered in a medium solution co-incubated with the cells for 24 h. For the ACMF group, the cells were thermally treated for 10 min with a magnetically induced hyperthermia apparatus, and the medium was removed. The cells were fixed with 2.5% room temperature glutaraldehyde fixative for 5 min. In addition, the cells were gently hung down in one direction with a cell scraper, transferred to a 15-mL centrifuge tube with a pasteurized pipette, and centrifuged at 3000 rpm/2 min. Then, the fixative was discarded and added with a new electron microscopy fixative for 30 min at room temperature and protected from light. The mitochondrial morphology of cells was observed and photographed by TEM.

Hemolytic reactions

A total of 2 mL of blood was collected from the eyes of 6- to 8-week-old female Balb/c mice and placed in an anticoagulant tube. The blood was centrifuged (3000 rpm, 15 min), and red blood cells were collected. Then, 0.1 mL of erythrocyte suspension was mixed with different concentrations (25, 50, 75, and 100 μg/mL) of gel and Fe3O4@Gel, and different concentrations (0.05, 0.1, 0.2, 0.4 μg/mL) of AS4S4@Gel and AS4S4/Fe3O4@Gel, and incubated at 37 °C for 4 h. The samples were then centrifuged at 3000 rpm for 15 min. The results were recorded by taking photographs. Erythrocytes were mixed with ddH2O for a 100% hemolysis control. After centrifugation of the samples, the absorbance of the supernatant was tested at 542 nm using an automated enzyme marker (Thermo Fisher Scientific). Percent hemolysis was calculated using the following equation:

$$\text{Hemolysis}(\%) = \left(I/I0\right) \times 100\%,$$

where I denotes the absorbance value of the experimental group, and $I0$ denotes the absorbance value of erythrocytes after complete hemolysis in ddH2O.

In vivo magnetic-thermal properties

To explore the in vivo photothermal properties of AS4S4/Fe3O4@Gel, a subcutaneous transplantation tumor model was established by subcutaneous inoculation of 0.1 mL of Lewis cell suspension (1×10^8 cells/mL) into the axilla of the left front leg of female Balb/c mice. When the tumor volume reached 100 mm^3, based on the equation: tumor volume (mm^3) = 1/2 × length × (width)^2, the tumor was injected with a single injection of 100 ul AS4S4/Fe3O4@Gel (5 mg/kg), and the tumor of the mice was treated with a magnetic induction thermotherapy instrument for 30 min (power of 390 kHz/2.58 Kam). Temperature changes during irradiation were recorded using infrared thermography (HIKORO K20 camera, Hangzhou, China). This camera captures infrared radiation emitted by objects and converts it into visual images, enabling the detection of temperature distributions and other conditions of the objects.

Fluorescence imaging

To evaluate the fluorescence imaging effect of AS4S4/Fe3O4@Gel in solid tumors in vivo, we chose subcutaneous transplantation of lung carcinoma in Balb/c mice at 6–8 weeks after body hair removal as a model. We injected 200 μL of AS4S4/Fe3O4@Gel (5 mg/kg) via a single intratumoral injection, followed by immediate placement of the injected tumor into the magnetic induction hyperthermia machine for 30 min (with a power of 390 kHz/2.58 Kam). In addition, the AS4S4/Fe3O4@Gel control administration group was set simultaneously at the same dose. The fluorescence signals in the tumor region were monitored in situ in real time after injection using a small animal in vivo fluorescence imaging system at different time intervals of 12, 24, 36, 48, 60, and 72 h (excitation wavelength Ex was set to 570 nm, and emission wavelength Em was set to 680 nm) (He et al. 2020).

Blood and biochemical indicators

To study the effect of AS4S4/Fe3O4@Gel on the indicators of blood and liver and kidney functions in Balb/c loaded mice, we took whole blood and serum of the mice after 15 days of drug administration and examined them. Blood indices and liver and kidney function indices were tested.

In vivo antitumor effects

To assess the combined antitumor efficacy of AS_4S_4/Fe_3O_4@Gel and ACMF in vivo, we utilized a model of subcutaneously transplanted lung cancer in 6- to 8-week-old female Balb/c mice. Specifically, 100 μL of a cell suspension containing 1×10^6 Lewis lung carcinoma cells was injected into the posterior region of their right legs**.** A total of 60 mice were involved in this study. After confirming cancer cell survival in the nude mice, we regularly measured the tumor's length and width using a vernier caliper. Tumor volume was then estimated using the formula: volume = [length * $(\text{width})^2$]/2. When the tumor volume reached 100 mm^3, mice were randomly divided into 7 groups: (1) blank control group, (2) Gel group, (3) ACMF group, (4) AS_4S_4@Gel + ACMF group, (5) AS_4S_4/Fe_3O_4@Gel group, (6) Fe_3O_4@Gel + ACMF group, and (7) AS_4S_4/Fe_3O_4@Gel + ACMF group (each group contained at least 8 mice). For the (2) group of tumor-bearing mice, a single intratumoral injection of 100 μl Gel was administered; for the (4) group of tumor-bearing mice, a single intratumoral injection of 100 μl AS_4S_4@Gel was administered, resulting in a drug concentration of 4.5 mg/kg AS per mouse; for the (6) group of tumor-bearing mice, a single intratumoral injection of 100 μl Fe_3O_4@Gel was administered, resulting in a drug concentration of 25 mg/kg Fe per mouse; for the (5, 7) groups of tumor-bearing mice, a single intratumoral injection of 100 μl AS_4S_4/Fe_3O_4@Gel was administered, resulting in a drug concentration of 4.5 mg/kg AS and 25 mg/kg Fe per mouse; meanwhile, mice in the combined ACMF group (4, 6, 7) were anesthetized with isoflurane using a small animal gas anesthesia machine, and underwent magnetic induction hyperthermia treatment for 30 min at a power of 390 kHz/2.58KA $\times$ M^{-1}, with treatment administered every other day. Starting from the day of intratumoral drug injection, the tumor volume and mouse body weight were measured every 2 days for a total of 14 days. On the second day after the end of treatment, mice were anesthetized using a gas anesthesia machine and then killed by cervical dislocation. The tumor tissues, heart, liver, lungs, kidneys, and other organs were quickly removed. These organs were fixed in 4% paraformaldehyde and stored at room temperature, then were stained with H&E, immunohistochemistry (IHC), and TUNEL. Experimental animals were kept in SPF environment.

Statistical analysis

The data were generated using GraphPad Prism 9.0 Project software. One-way analysis of variance or unpaired tests were used to assess the differences between the groups. The results are presented as mean ± standard error. $P < 0.05$ was considered a statistically significant difference.

Results

Characterization of AS4S4/Fe3O4@Gel

The morphology of Fe3O4@DMSA and AS4S4 was characterized using TEM, as revealed in Fig. 1Ai. Notably, Fe3O4 is spherical with a uniform particle size, and the

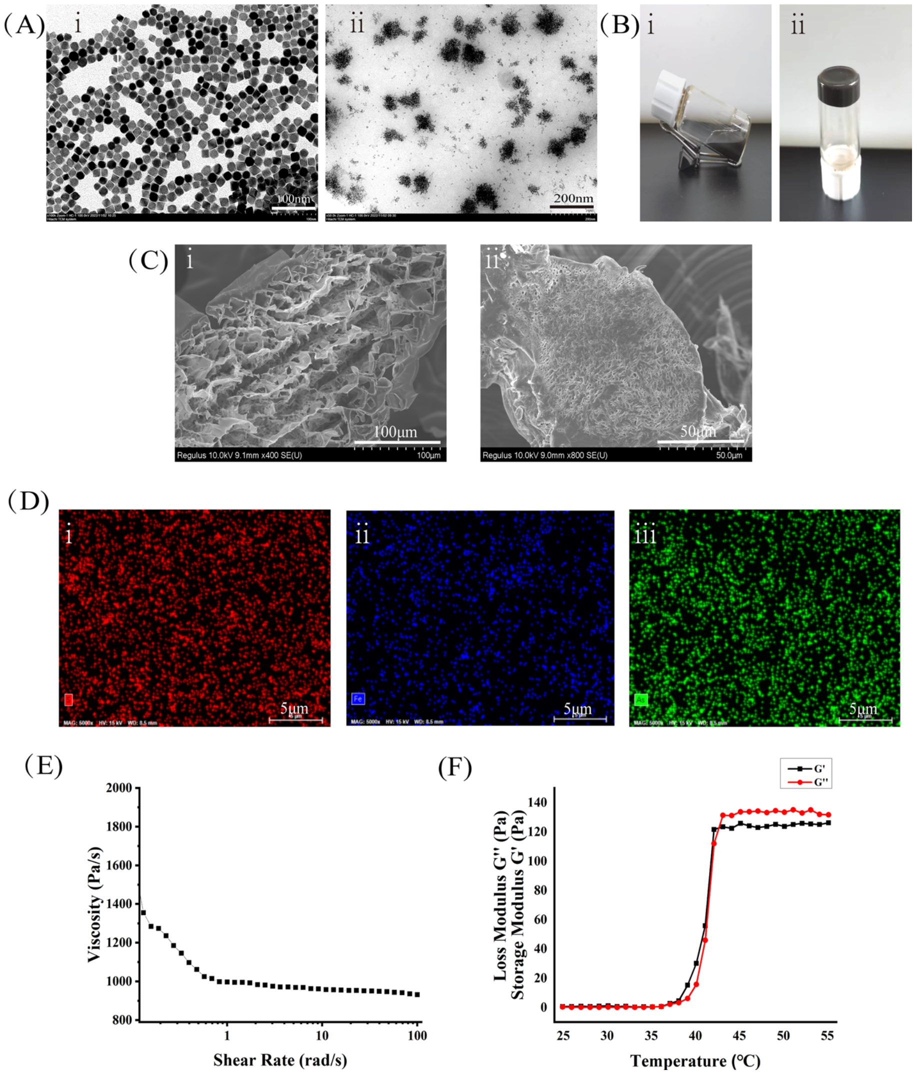

Fig. 1 **A** Transmission electron micrographs of Fe3O4@DMSA and AS4S4; **B** graphs of glass transition temperature determined by inversion method; **C** scanning electron microscope graphs of blank and loaded hydrogels; **D** graphs of elemental analyses of S, Fe, and AS; **E**, **F** graphs of rheological properties of loaded hydrogels

individual particle size is around 20 nm. As presented in Fig. 1Aii, AS4S4 is in the form of clusters of varying sizes, with individual clusters of about 150 nm.

The SEM results revealed that the hydrogel has a three-dimensional mesh structure with many holes, as illustrated in Fig. 1Ci and ii, which is helpful for the encapsulation and release of the drug at a later stage. XPS were often used to analyze the chemical valence and relative content of elements on the surface of materials. For AS_4S_4/Fe_3O_4@Gel, the chemical states of As, S, Fe and other elements can be determined by XPS, and the relative content of each element on the surface can be inferred from the relative proportion of the peak area. This is important for studying the surface properties and composition distribution of the material, and also helps to verify that the stoichiometric relationships inside and on the surface of the material are consistent. Elemental analyses of the Fe, As, and S elements demonstrated in Fig. 1Di–iii confirmed that the drug-carrying hydrogel was successfully coated with Fe3O4 and AS4S4.

The relationship between hydrogel shear rate and viscosity showed that the hydrogel viscosity decreased with the increase of shear rate, as illustrated in Fig. 1E. To further verify the hydrogel phase transition temperature, hydrogel modulus storage and loss changes were detected at different temperatures, as indicated in Fig. 1F. The data showed that between 25 and 35 °C, the modulus storage G' and modulus loss G" of the samples did not change significantly, indicating that the samples presented a solution with good fluidity. When the temperature reaches 42 °C, the sample becomes a solid colloid, which is the gel point.

To detect changes in the gel state of the hydrogel at different temperatures, the physical state of hydrogel was examined at room and gel point temperatures, and the results showed that the temperature-sensitive hydrogel demonstrated good flowability at room temperature. When the temperature was increased to the gel point (42 °C), the hydrogel was an immobile semi-solid gel state, as displayed in Fig. 1Bii, aligning with the above phenomenon of the change of storage modulus and modulus of loss with temperature.

The fluorescence emission peaks of the materials were detected by fluorescence spectroscopy. The results revealed that the group containing the AS4S4 ingredient exhibited a distinct fluorescence emission peak at 570 nm, as disclosed in Fig. 2A, C, E and analyzed using the UV spectrophotometer, which showed that the group with the AS4S4 ingredient displayed a distinct UV absorption peak at around 450 nm, as indicated in Fig. 2B, D, F. This could pave the way for integrating in vivo diagnosis and treatment.

The ICP we choose is sequential scanning ICP, whose quantitative analysis accuracy of elements can reach a very high level when detecting trace impurity elements in electronic grade chemicals, it can be accurate to ppm (one part per million) or even ppb (one part per billion) level, and it can detect a variety of elements including metal and non-metal elements. From common metal elements such as iron, copper, zinc, to non-metallic elements such as sulfur, silicon, phosphorus, etc., can be effectively detected, covering most of the elements in the periodic table. Using ICP to detect the drug release rate of the hydrogel at different temperatures, as displayed in Fig. 3A, it can be seen that the drug release rate of the hydrogel at 42 °C was significantly higher than that at 37 °C, confirming that the drug release rate of our synthesized hydrogel was temperature-dependent.

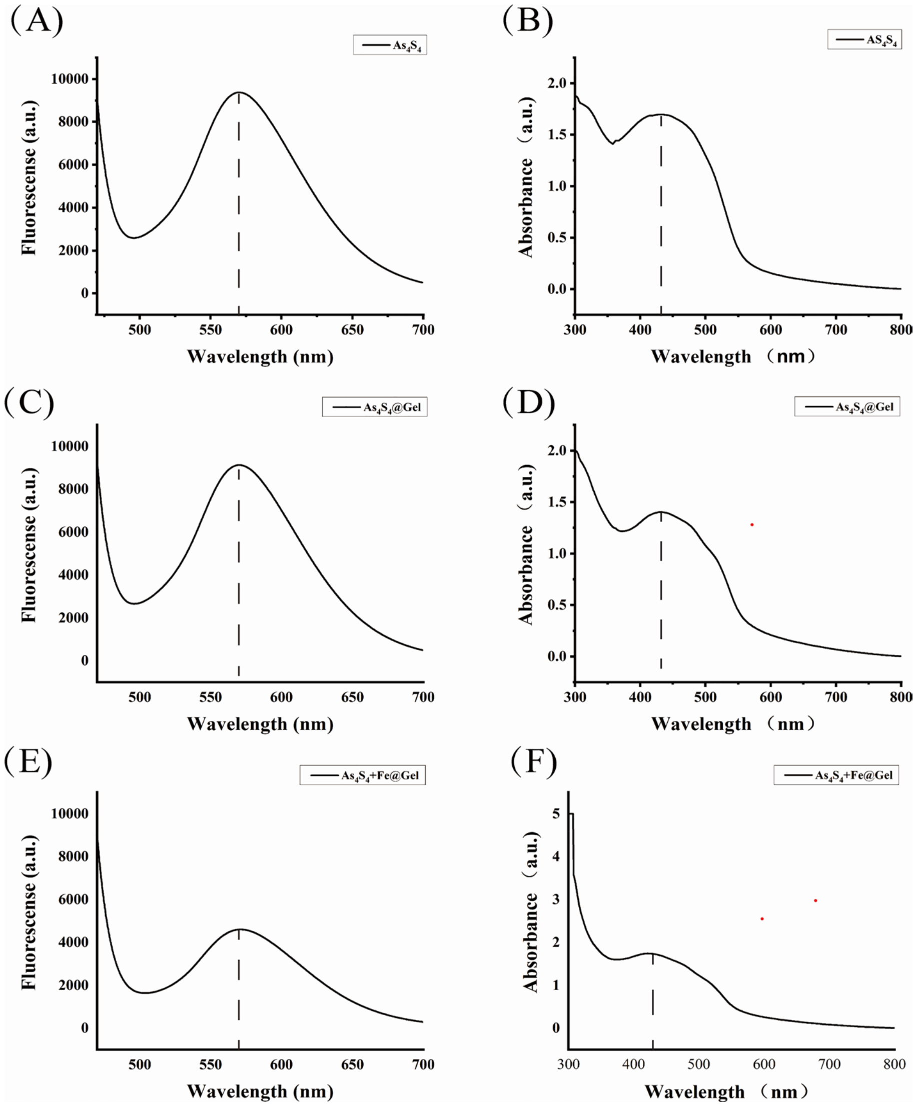

Fig. 2 **A**, **C**, and **E** Fluorescence emission spectra of AS4S4, AS4S4@Gel, and AS4S4/Fe3O4@Gel; and **B**, **D**, and **F** ultraviolet absorption spectra of AS4S4, AS4S4@Gel, and AS4S4/Fe3O4@Gel

According to the pyrogen test results, the temperature rise of all rabbits did not exceed 0.6 °C, and no pyrogen reaction symptoms were found, it was concluded that the AS_4S_4/Fe_3O_4@Gel formula passed the pyrogen test.

In vitro and in vivo biocompatibility measurements

Although past studies have concluded that hydrogels are biocompatible, assessing whether synthetic materials are biosafe is also necessary. Using the CCK-8 assay to assess their cytotoxicity, Lewis cells and A549 cells were co-cultured with various concentrations (5, 10, 20, 40, 80, and 100 μg/mL) of gel for 24 h. As presented in Fig. 3B, after treating the cells with 100 μg/mL of gel, cell viability was higher than 85%, and cytotoxicity was very low.

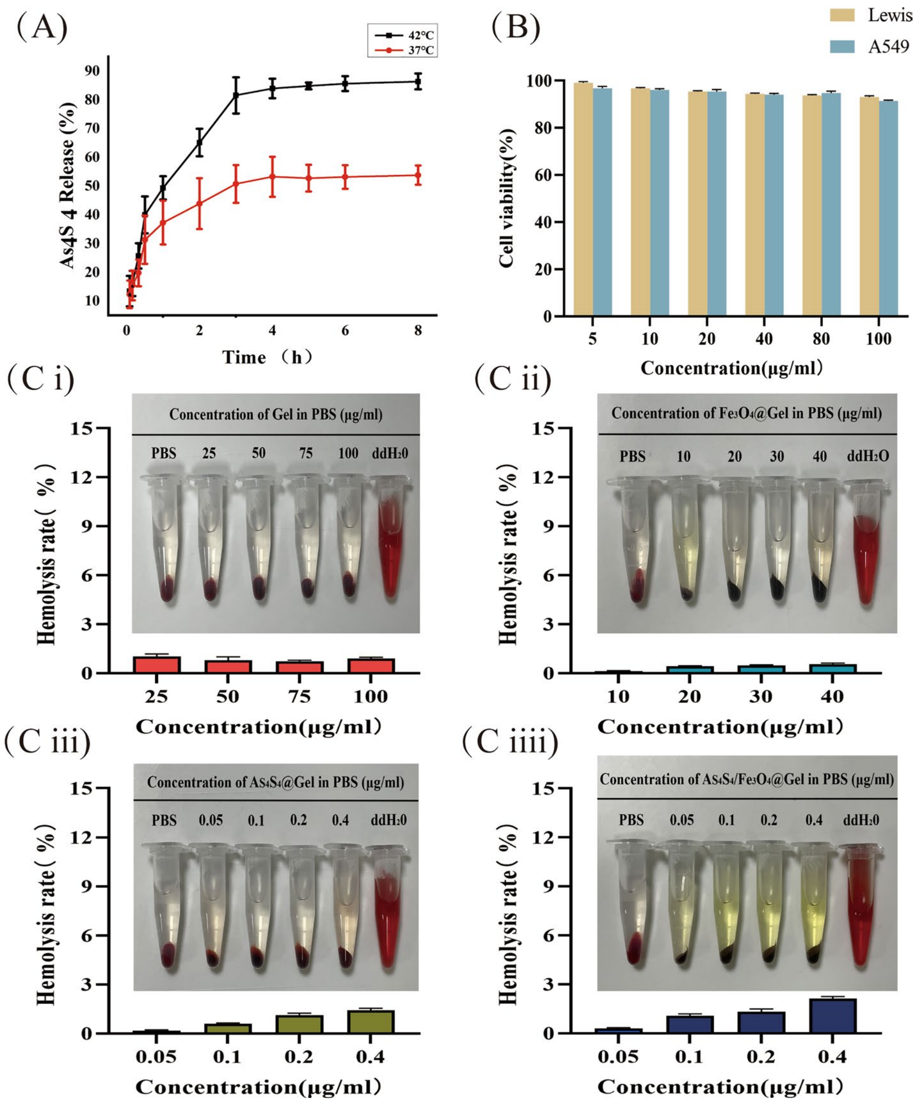

Fig. 3 **A** Drug release rate of drug-loaded hydrogel; **B** cell viability of Lewis and A549 cells in different concentrations of unloaded hydrogel; C hemolysis assay with varying concentrations of Gel, AS4S4@Gel, Fe3O4 @Gel, and AS4S4/Fe3O4@Gel

Hemolysis is caused by the rupture of red blood cells, releasing hemoglobin into the surrounding fluid. Therefore, hemolytic reactions are commonly used to assess the blood compatibility of materials. As displayed in Fig. 3Ci–iiii, minimal hemoglobin release was observed from mouse erythrocytes treated with gel, AS4S4@Gel, Fe3O4@Gel, and AS4S4/Fe3O4@Gel. Very few erythrocytes were destroyed compared to erythrocytes treated with ddH2O. The hemolysis rate at different drug concentrations was less than 3%, indicating that the nanomaterials showed satisfactory biocompatibility with mouse erythrocytes.

Fluorescence imaging and magneto-thermal effects

To further evaluate AS4S4/Fe3O4@Gel tumor diagnostic and therapeutic effects at the in vivo level, we established subcutaneous Lewis lung cancer cell transplantation tumors in mice as an animal model to study the fluorescence and magneto-thermal effects produced under AS4S4/Fe3O4@Gel chemotherapy combined with ACMF. First, we investigated the enrichment, body degradation, and metabolism of locally administered AS4S4/Fe3O4@Gel in the tumor by a small animal in vivo fluorescence imaging system. The results are presented in Fig. 4A. With the prolongation of the time of AS4S4/Fe3O4@Gel in the tumor, the fluorescence signal intensity in the tumor region of mice was strengthened. The value of the fluorescence signal reached its highest at 12 h, then the fluorescence signal gradually decayed in the subsequent 12–72 h process, and the fluorescence signal gradually weakened. In addition, the fluorescence signal in the tumor region after the administration of the same dose of AS4S4/Fe3O4@Gel was significantly weaker than the fluorescence intensity of AS4S4/Fe3O4@Gel + ACMF at the same time point, confirming that our synthesized hydrogel exhibited a slow-release effect in mice and prolonged the time of the drug in the tumor.

Moreover, Balb/c loaded mice were used to study the magneto-thermal effect of AS4S4/Fe3O4@Gel. Notably, AS4S4/Fe3O4@Gel was injected into the tumor of mice. The mice were placed in a magnetic induction thermotherapy apparatus for 30 min to compare the photothermal images of the tumor tissues at different time points. As presented in Fig. 4B, exposure to the alternating current (AC) magnetic field can rapidly increase the temperature of the tumor tissues and reach the gel point of about 42 °C in about 9 min. This can cause AS4S4/Fe3O4@Gel to change from the liquid state to the gel state, allowing for better control of the range of the drug release in the hydrogel.

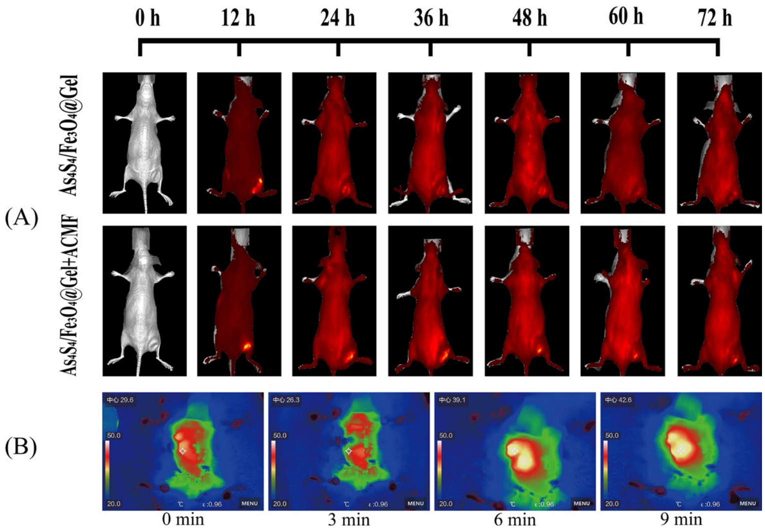

Fig. 4 **A** Fluorescence imaging in mice injected intratumorally with AS4S4/Fe3O4@Gel 12–7 h mice; **B** magneto-thermal effect in mice injected intratumorally with AS4S4/Fe3O4@Gel 0–9 min

Cancer cell proliferation, apoptosis, and iron death in vitro

The excellent biocompatibility and superior magneto-thermal effect prompted us to further explore its potential application in anticancer drugs. Lewis cells were co-cultured with different concentrations of AS4S4@Gel, Fe3O4@Gel, and AS4S4/Fe3O4@Gel medium solutions for 24 h. The results were detected using the CCK-8 kit, which showed that the IC50 value of AS4S4@Gel was 0.11 μg/mL, Fe3O4@Gel demonstrated an IC50 value of 36 μg/mL, and AS4S4/Fe3O4@Gel indicated an IC50 value of 0.09 μg/mL.

To study the effect of AS4S4/Fe3O4 @Gel cell proliferation. We used an EdU-488 kit to detect cells treated with IC50 drug concentration and magnetic induction thermotherapy. The fluorescent dye EdU-488 reacted specifically with proliferating cells to produce red fluorescence. As illustrated in Figs. 5 and 7C, the AS4S4/Fe3O4@Gel + ACMF group (Fig. 5F) showed a significant reduction ($P < 0.05$) in red fluorescence compared to AS4S4/Fe3O4@Gel (Fig. 5D). The results indicated that ACMF resulted in more AS4S4/Fe3O4@Gel dedicated cell proliferation inhibition ($P < 0.01$).

Apoptosis was found to be an important mechanism for the antitumor activity of antitumor drugs. We evaluated the killing effect of AS4S4/Fe3O4@Gel (dose 0.1 μg/mL) on Lewis cells by early and late apoptotic cell rates using flow cytometry with FITC-Annexin V/PI dual fluorescent labeling. As shown in Fig. 6A, the apoptosis rate induced by AS4S4/Fe3O4@Gel group and AS4S4/Fe3O4@Gel + ACMF group was significantly higher than that of the other groups. The overall apoptosis rate of the Lewis cells after AS4S4/Fe3O4@Gel was increased from 2.52% to 22.12%, and the apoptotic rate of the cells increased by 55.5% in combination with ACMF, suggesting that the apoptotic rate of ACMF increased from 2.52 to 22.12%, indicating that ACMF can effectively improve the apoptosis of lung cancer cells. Meanwhile, the Gel and ACMF groups showed the same trend as the control group, with apoptosis rates of 1.83% and 2.33%, respectively, indicating that Gel and ACMF alone could not promote the apoptosis of tumor cells.

To further understand the mechanism of action of AS4S4/Fe3O4@Gel in tumor cells, we performed proteomics analysis, which is based on mass spectrometry technology to analyze proteins in living organisms and is crucial in studying biological processes and drug action mechanisms. As displayed in Fig. 6B, the expression of apoptosis-related protein bcl-2 was significantly reduced in the AS4S4/Fe3O4@Gel group and AS4S4@

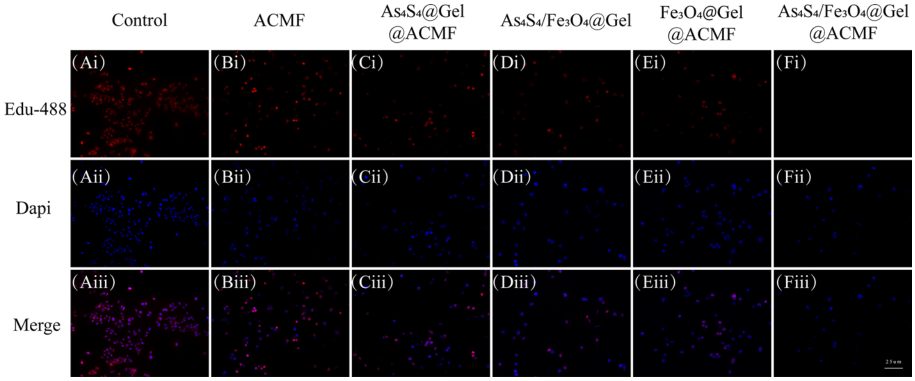

Fig. 5 EdU-488 cell proliferation assay of cells after different treatment groups

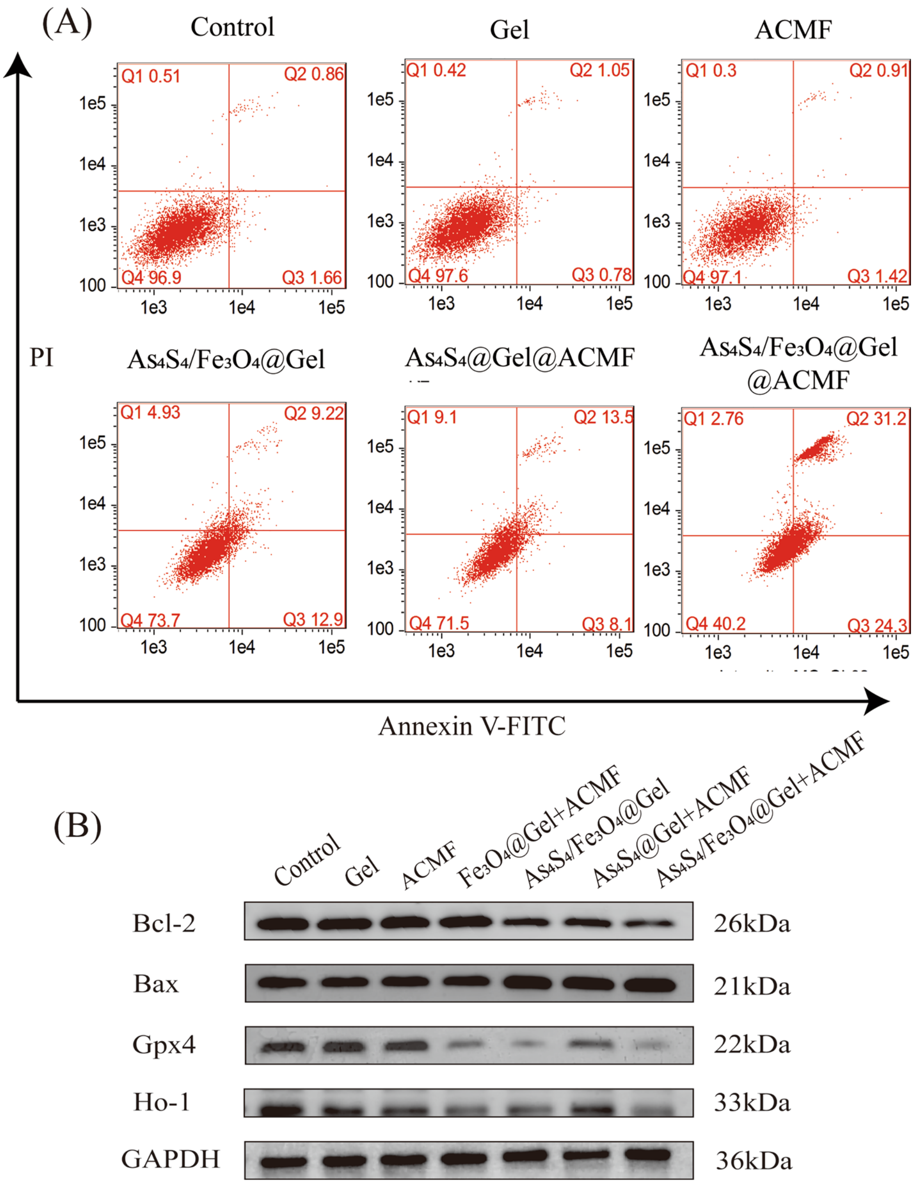

Fig. 6 **A** Flow apoptosis map of FITC-Annexin V/PI after different groups of treatments; **B** Western blot protein blot of different treatment groups

Gel group, while the expression of the corresponding proteins in the cells in the combined ACMF group showed the lowest expression trend. Meanwhile, Bax protein expression showed the opposite trend. This indicates that Bcl-2 and Bax are crucial in AS4S4/Fe3O4@Gel-induced apoptosis, which aligns with the results of Zong et al. (Li et al. 2022). In the Fe3O4@Gel and AS4S4/Fe3O4@Gel groups, the expression of iron death-related proteins GPX4 and HO-1 was significantly reduced ($P<0.05$), while the expression of the corresponding proteins in the cells was the lowest in the combined ACMF group ($P<0.01$). This not only indicates that AS4S4/Fe3O4@Gel can induce iron death, but also suggests that combined ACMF can promote iron death. Based on previous reports (Zhang et al. 2024, 2022; Liu et al. 2022), realgar induces cellular iron death. Comparing the AS4S4@Gel combined ACMF group with the ACMF group, the

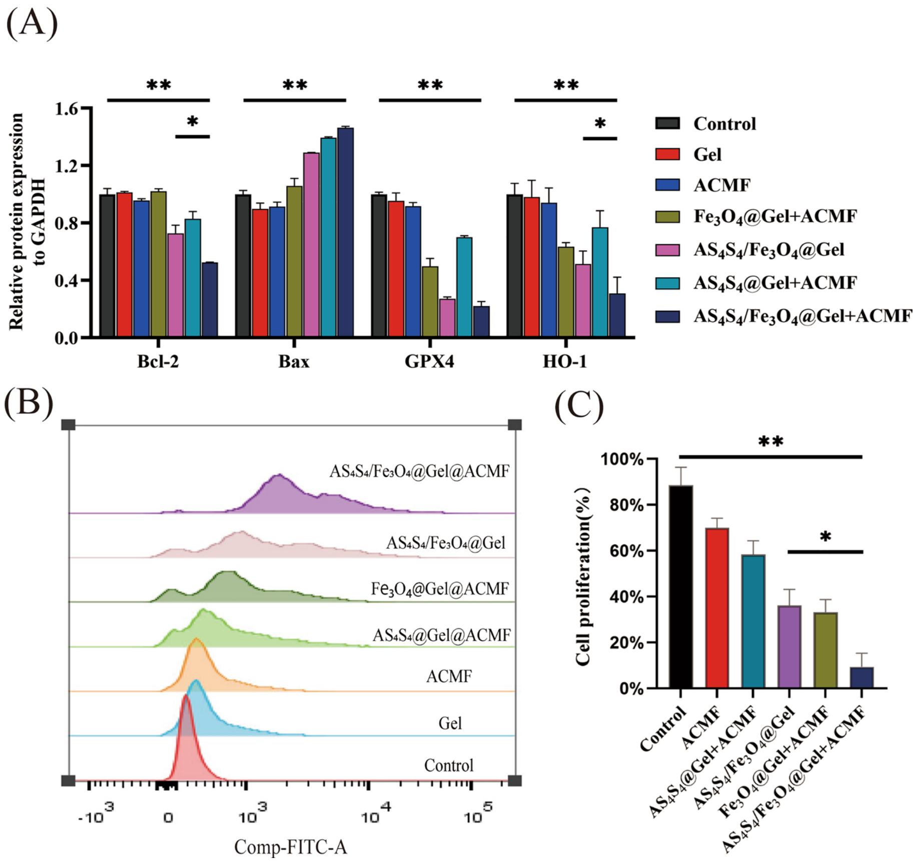

Fig. 7 **A** Statistical analysis of protein expression of Bcl-2, Bax, GPX4, and Ho-1 relative to GAPDH; **B** the ROS content of cells in different groups of treatments; **C** statistical analysis of cell proliferation of cells EdU-488 after different treatment groups

expression of GPX4 and HO-1 was decreased. This suggests that AS4S4 promotes iron death of lung cancer cells by decreasing the expression of GPX4 and HO-1 proteins (Fig. 7A).

It was found that iron death can lead to an increase in intracellular ROS (Yang et al. 2022; Kang et al. 2023). To validate our conjecture further, we performed a probe assay with DCFH-DA, and the staining results, as illustrated in Fig. 7B, showed that AS4S4/Fe3O4@Gel group slightly increased ROS, whereas AS4S4/Fe3O4@Gel + ACMF induced a large increase in ROS. Meanwhile, as depicted in Fig. 8, TEM results revealed that compared with the negative control group, the mitochondrial membrane density of lung cancer cells was increased in the AS4S4/Fe3O4@Gel treated group. However, the mitochondrial membrane density of lung cancer cells was further increased, and the volume became smaller in the AS4S4/Fe3O4@Gel combined with the ACMF group. It was confirmed that the AS4S4/Fe3O4@Gel combined with ACMF did promote iron death.

In vivo inhibition of lung cancer by AS4S4/Fe3O4@Gel

As displayed in Fig. 9A, B, AS4S4/Fe3O4@Gel combined with ACMF significantly inhibited tumor growth compared with other control groups. Mice treated with ACMF alone showed a rapid increase in tumor tissue. In the absence of an AC magnetic field,

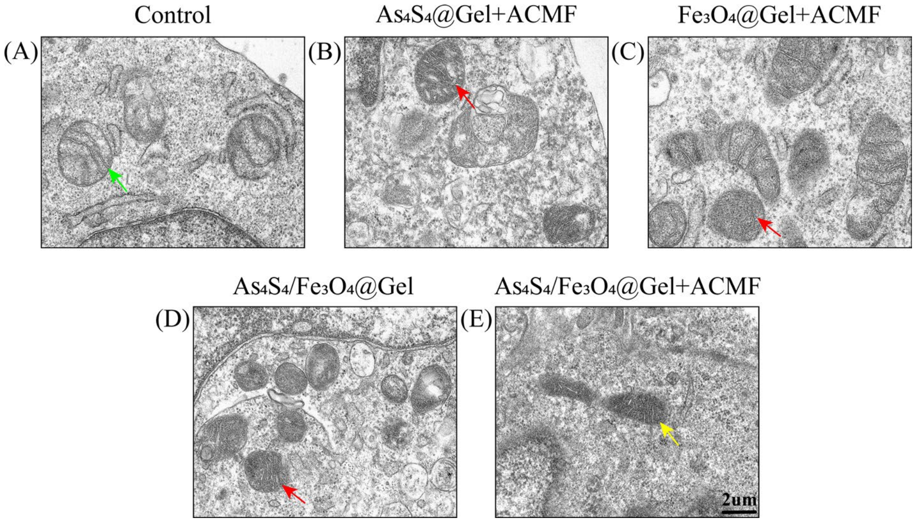

Fig. 8 Mitochondrial morphology of lung cancer cells after treatment with different groups (green arrows represent normal mitochondrial structure, red arrows represent increased mitochondrial membrane density, and yellow arrows represent increased mitochondrial membrane density and reduced mitochondrial size)

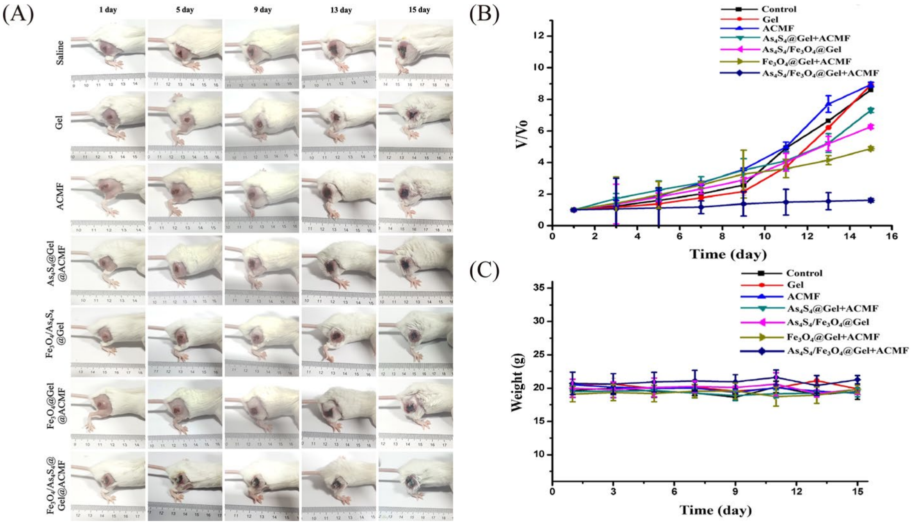

Fig. 9 **A** Photographs of tumors in different groups of treated mice; **B** tumor growth curves; **C** changes in body weight of mice carrying Lewis tumor Balb/c recorded every other day after different treatments

AS4S4/Fe3O4@Gel partially inhibited tumor growth. In addition, an enhanced therapeutic effect was observed by treating AS4S4/Fe3O4@Gel with ACMF compared to no ACMF. This may be because ACMF increased the magnetic induction thermotherapy of the tumor tissue in the presence of Fe3O4 @Gel while triggering the release of AS4S4@ Gel inside the temperature-sensitive hydrogel material.

To further investigate the antitumor mechanisms induced by AS4S4/Fe3O4@Gel combined with ACMF treatment, we utilized commonly used histopathological methods such as immunohistochemistry and TUNEL to assess proliferation, migration, neovascularization, apoptosis, and iron death of the tumor cells. Notably, Ki-67, a nuclear protein marking cell proliferation, and CD31, also known as platelet-endothelial cell adhesion molecule protein, were used to assess tumor angiogenesis. It demonstrated a close relationship with tumor neovascularization in the process of tumor development, progression, and prognosis; E-cadherin, called calcium adhesion protein E, is crucial in tumor cell invasion. As presented in Fig. 10, from the tissue sections, compared with the saline, gel, and ACMF groups, the expression of ki-67 in the AS4S4/Fe3O4@Gel administration group and the combined ACMF treatment group was significantly reduced, indicating that the two treatments can effectively inhibit the proliferation of tumor cells. In addition, CD31 expression in these two groups was significantly down-regulated, indicating that the AS4S4/Fe3O4@Gel and the combined treatment can inhibit the generation of tumor neovascularization. Meanwhile, Bcl-2 and GPX4 protein expression could indicate that these two groups of treatments induced apoptosis and iron death of tumor cells, corresponding to the cell in vitro experiments. In comparison, the antitumor effect of the combination treatment group was stronger than that of the single AS4S4/Fe3O4@Gel administered group. In TUNEL staining, we can study the apoptosis of tumor cells after the administration of each group. From the figure, the nuclei of the tumor cells in the AS4S4/Fe3O4@Gel administration group and the combined treatment group were brownish and showed nuclear rupture, chromatin crumpling, and fragmentation of the cells, which displayed obvious apoptotic morphology. Meanwhile, there were only a small number of brown apoptotic cells in the saline, Gel, and ACMF groups, indicating that the AS4S4/Fe3O4@Gel administration group combined with the ACMF group demonstrated significant antitumor ability.

In addition, to validate the in vivo biosafety AS4S4/Fe3O4@Gel, we analyzed the body weight changes and important tissue H&E staining data in mice. As presented in Fig. 9C, no significant change was observed in the body weight of the hormonal mice before and after treatment. As displayed in Fig. 11, the H&E-stained sections of tissues of the heart, liver, spleen, lung, kidney, and other organs in different groups were normal and showed no damage. Tumor tissue sections showed fragmented nuclei, incomplete cell structure,

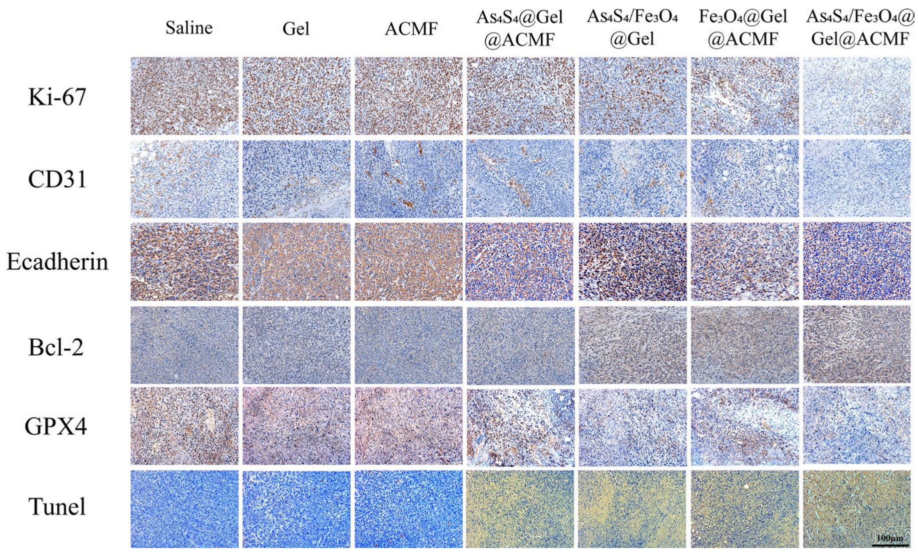

Fig. 10 Immunohistological analysis and TUNEL apoptosis staining in different groups of treated mice

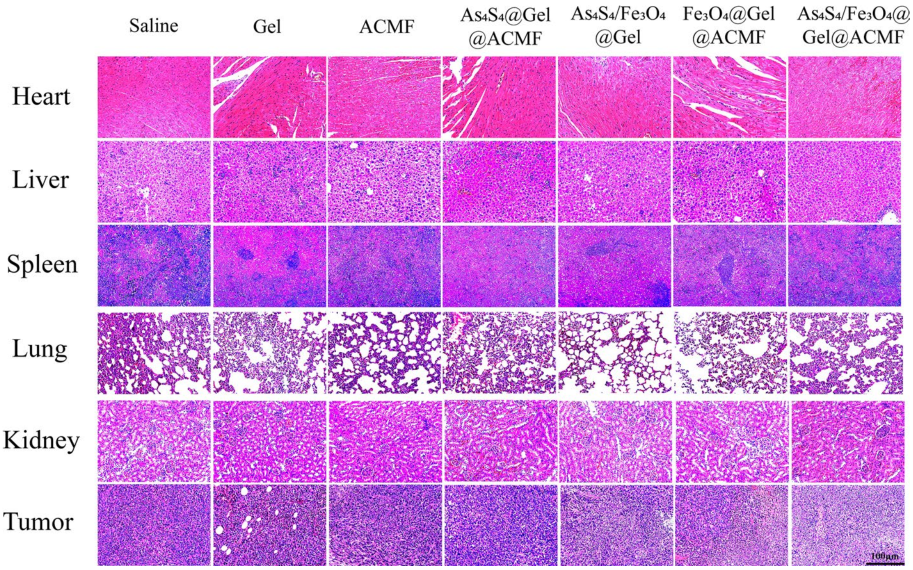

Fig. 11 The H&E staining of heart, liver, spleen, lungs, kidneys, and tumors in different groups of treated mice 15 days after treatment

and nucleoplasmic separation, indicating that AS4S4/Fe3O4@Gel exerted antitumor effects without causing damage to other organs of mice and toxic side effects. Meanwhile, as displayed in Fig. 12A, blood routine testing indicators (WBC, RBC, HGB, HCT, MCV, MCH, MCHC, and PLT) and, as presented in Fig. 12B, liver and kidney function indicators (AST, ALP, ALT, BUN, and CREA) were maintained at normal levels. This confirms that AS4S4/Fe3O4@Gel has better biosafety and is expected to be a good medicine for lung cancer treatment.

Discussion

Injectable temperature-sensitive hydrogels are an attractive drug delivery system that undergoes a sol–gel phase transition with temperature changes after injection. Recently, temperature-sensitive hydrogels have become an essential component of oncology therapy due to their high local drug concentration, slow release, and low systemic toxicity. It can also deliver various therapeutic agents for different tumor treatment modalities, including chemotherapy, photothermal therapy, photodynamic therapy, gene therapy, combined chemo–photothermal therapy, and combined chemo–immunotherapy (Xiao et al. 2021).

Research on AS4S4 and iron oxide applications is extensive. However, combining nanorealgar and nanoiron oxide with temperature-sensitive hydrogel technology for encapsulated chemotherapy and magnetically induced thermotherapy, along with simultaneous fluorescence and magnetically induced imaging, is relatively new. Therefore, we developed a drug release system for local injection of temperature-sensitive hydrogels for tumor monitoring, which can simultaneously deliver antitumor drugs to the tumor site for tumor monitoring.

Based on material characterization results, this temperature-sensitive drug release system demonstrated good temperature sensitivity and achieved good controlled release at

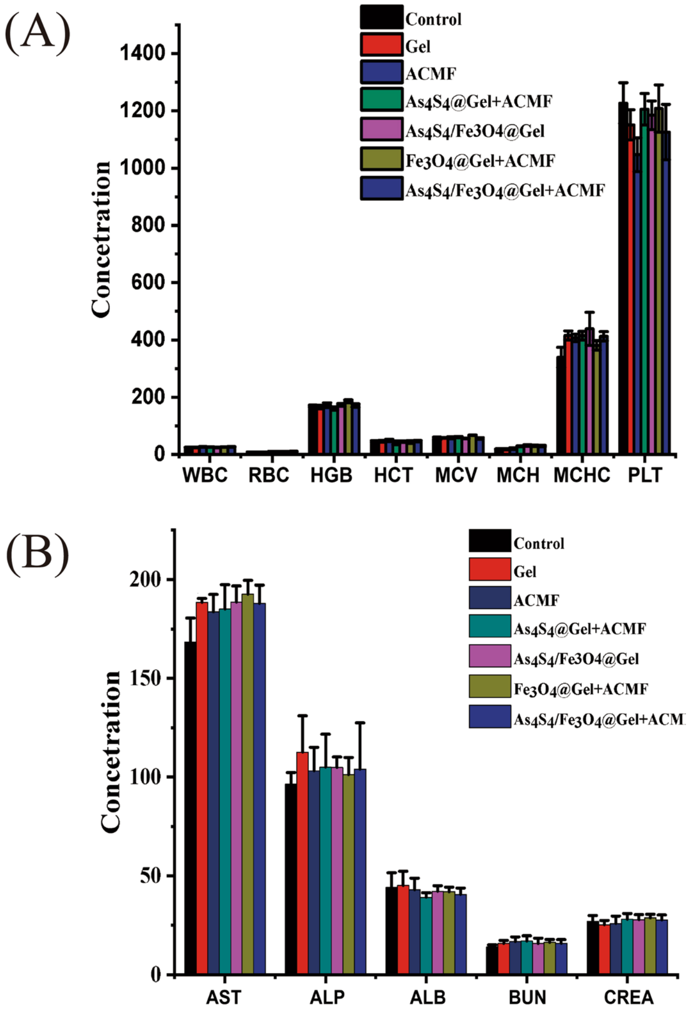

Fig. 12 **A**, **B** Blood routine and biochemical indexes of different groups of treated mice 15 days after treatment

the site of action. The biocompatibility of AS4S4/Fe3O4@Gel has been proven by cytotoxicity and hemolytic reaction. The results of in vitro experiments showed that AS4S4/Fe3O4@Gel combined with the ACMF group inhibited tumor cell proliferation better than AS4S4/Fe3O4@Gel alone group and induced more apoptosis and iron death of tumor cells. In Lewis transplantation tumors, AS4S4/Fe3O4@Gel also showed an excellent magneto-thermal effect, while AS4S4/Fe3O4@Gel combined with ACMF exhibited a better antitumor effect than chemotherapy alone.

Although the potential of temperature-sensitive hydrogels has been successfully demonstrated in vitro, further studies are needed to confirm whether they fulfill the long-term efficacy and safety requirements for clinical applications. In addition, the synthesis of nanorealgar and iron oxides is still in the laboratory stage, and further exploration is needed to optimize the formulation and design of nanorealgar and hydrogels to maximize their therapeutic potential for large-scale applications in biomedicine. For lung cancer, the primary tumor has a certain degree of mobility. If the injection time is too long, gel may harden. The pulmonary capillaries are abundant and have alveolar structures, which may easily lead to the loss of thermal generated by nanomaterials, affecting the therapeutic effect. Therefore, predicting patients with cervical lymph node metastasis is more suitable for our study. In addition, our study did not clarify the contribution of different components and treatment modes of the nanomaterial to the antitumor effect. In this article, we also did not investigate the degradation of nanomaterials or their impact on drug release and antitumor efficacy. Finally, the magnetic resonance imaging capabilities of hydrogel-encapsulated iron oxide still need to be explored in subsequent experiments. Therefore, these shortcomings require further research and discovery in the future.

Conclusion

This study synthesized a series of morphologically realgar nanocrystals and encapsulated AS4S4 and Fe3O4 with a temperature-sensitive hydrogel with good biocompatibility. The AS4S4/Fe3O4@Gel is a locally injectable therapeutic platform with satisfactory temperature sensitivity, a high drug-controlled release rate, certain fluorescence properties, and good hemocompatibility. In particular, AS4S4/Fe3O4@Gel combined with ACMF showed ideal antitumor efficacy in lung cancer models and inhibited tumor progression by inducing apoptosis and iron death. Overall, this study demonstrated that nanohydrogels are simple to prepare, and their chemotherapeutic and magnetic induction thermotherapy properties have great potential in the clinical treatment of lung cancer.

Acknowledgements

We appreciate the design and construction of nanomaterial, as well as research technical support and the polishing services provided by the LEVIN (Wuhan) Institute of Biomedical Research (www.laierwen.com).

Author contributions

JT, RMD and MYW conducted the experiments. HZL, MJ, ZHJ, HZF and WGM designed the study. Technical assistance is provided by GB, SSL, LF and ZXY. JT and MYW wrote this paper. HJW, JT, HZF and RMD carried out the data analysis and submitted and revised the manuscript. HJW, HZL and WGM provided financial support. All authors read and approved the final paper.

Funding

The study were supported by the First Affiliated Hospital of Bengbu Medical University Science Fund for Distinguished Young Scholars (No. 2019BYYFYJQ04), Natural Science Research Project of Anhui Educational Committee (Nos. KJ2021A0692 and KJ2019A0313), Natural Science Foundation of Bengbu Medical University (No. 2023byzd059), and Research Funds of Joint Research Center for Regional Diseases of IHM (2024bydjk010).

Availability of data and materials

No datasets were generated or analysed during the current study.

Declarations

Ethics approval and consent to participate

This study was approved and supervised by the Animal Ethics Committee of Bengbu Medical University. All procedures strictly adhered to the guidelines for the care and use of laboratory animals established by Bengbu Medical University.

Competing interests

The authors declare no competing interests.

Received: 7 November 2024 Accepted: 17 February 2025

References

Abaei S, Tarighatnia A, Mesbahi A, Aghanejad A (2024) Antibody conjugates as CT/MRI Theranostics for diagnosis of cancers: a review of recent trends and advances. Sens Diagn 3(9):1428–1441

Barr T, Ma S, Li Z, Yu J (2024) Recent advances and remaining challenges in lung cancer therapy. Chin Med J (Engl) 137(5):533–546

Ding W, Ji T, Xiong W, Li T, Pu D, Liu R (2018) Realgar, a traditional Chinese medicine, induces apoptosis of HPV16-positive cervical cells through a HPV16 E7-related pathway. Drug des Devel Ther 12:3459–3469

Fan Q, Xiong W, Zhou H, Yang J, Feng J, Li Z, Wu L, Hu F, Duan X, Li B, Fan J, Xu Y, Chen X, Shen Z (2023) An AND logic gate for magnetic-resonance-imaging-guided ferroptosis therapy of tumors. Adv Mater 35(45):e2305932

Fernández-Acosta R, Iriarte-Mesa C, Alvarez-Alminaque D, Hassannia B, Wiernicki B, Djaz- Garcja AM, Vandenabeele P, Vanden Berghe T, Pardo Andreu GL (2022) Novel iron oxide nanoparticles induce ferroptosis in a panel of cancer cell lines. Molecules 27(13):3970

Fu JJ, Zhang JY, Li SP, Zhang LM, Lin ZX, Liang L, Qin AP, Yu XY (2018) CuS nanodot-loaded thermosensitive hydrogel for anticancer photothermal therapy. Mol Pharm 15(10):4621–4631

Gong D, Chen M, Wang Y, Shi J, Hou Y (2022) Role of ferroptosis on tumor progression and immunotherapy. Cell Death Discov 8(1):427

Guan H, Xu Y, Ma C, Zhao D (2022) Pharmacology, toxicology, and rational application of cinnabar, realgar, and their formulations. Evid Based Complement Alternat Med 2022:6369150

He Z, Jiang H, Zhang X, Zhang H, Cui Z, Sun L, Li H, Qian J, Ma J, Huang J (2020) Nano-delivery vehicle based on chlorin E6, photodynamic therapy, doxorubicin chemotherapy provides targeted treatment of HER-2 negative, αvβ3-positive breast cancer. Pharmacol Res 160:105184

He Z, Zhang H, Xiao H, Zhang X, Xu H, Sun R, Li S (2024) Ubiquitylation of RUNX3 by RNA-binding ubiquitin ligase MEX3C promotes tumorigenesis in lung adenocarcinoma. J Transl Med 22(1):216

Hollow SE, Johnstone TC (2023) Realgar and arsenene nanomaterials as arsenic-based anticancer agents. Curr Opin Chem Biol 72:102229

Kang N, Son S, Min S, Hong H, Kim C, An J, Kim JS, Kang H (2023) Stimuli-responsive ferroptosis for cancer therapy. Chem Soc Rev 52(12):3955–3972

Li Z, Zhang R, Yin X, Li N, Cui S, Wang T, Tan X, Shen M, Guo Y, Wang J, Guo D, Xu R (2022) Realgar (As(4)S(4)), a traditional Chinese medicine, induces acute promyelocytic leukemia cell death via the Bcl-2/Bax/Cyt-C/AIF signaling pathway in vitro. Aging (Albany NY) 14(17):7109–7125

Liu C, Guo X, Ruan C, Hu H, Jiang BP, Liang H, Shen XC (2019) An injectable thermosensitive photothermal-network hydrogel for near-infrared-triggered drug delivery and synergistic photothermal-chemotherapy. Acta Biomater 96:281–294

Liu J, Zhang Y, Li Q, Feng Z, Huang P, Wang W, Liu J (2020) Development of injectable thermosensitive polypeptide hydrogel as facile radioisotope and radiosensitizer hotspot for synergistic brachytherapy. Acta Biomater 114:133–145

Liu X, Hai Y, Dong J, Xu L, Hou W, Su J, Ren W, Liu D (2022) Realgar-induced KRAS mutation lung cancer cell death via KRAS/Raf/MAPK mediates ferroptosis. Int J Oncol. https://doi.org/10.3892/ijo.2022.5447

Ma Y, Jiang T, Zhang R, Liu F, Song S, Zhang H, Huang J, He Z (2024) The application of 2d mxene nanosheet -based thermosensitive gel delivery system loaded with cisplatin and imiquimod for lung cancer. Int J Nanomed 19:4719–4733

Mohaghegh S, Tarighatnia A, Omidi Y, Barar J, Aghanejad A, Adibkia K, Yang J, Feng J (2022) Multifunctional magnetic nanoparticles for MRI-guided co-delivery of erlotinib and L-asparaginase to ovarian cancer. J Microencapsul 39(4):394–408

Shukla MK, Dubey A, Pandey S, Singh SK, Gupta G, Prasher P, Chellappan DK, Oliver BG, Kumar D, Dua K (2022) Managing apoptosis in lung diseases using nano-assisted drug delivery system. Curr Pharm des 28(39):3202–3211

Tabnak P, HajiEsmailPoor Z, Soraneh S (2021) Ferroptosis in lung cancer: from molecular mechanisms to prognostic and therapeutic opportunities. Front Oncol 11:792827

Tan W, Chen S, Xu Y, Chen M, Liao H, Niu C (2023) Temperature-sensitive nanocarbon hydrogel for photothermal therapy of tumors. Int J Nanomedicine 18:6137–6151

Tian Y, Wang X, Xi R, Pan W, Jiang S, Li Z, Zhao Y, Gao G, Liu D (2014) Enhanced antitumor activity of realgar mediated by milling it to nanosize. Int J Nanomed 9:745–757

Turrina C, Klassen A, Milani D, Rojas-González DM, Ledinski G, Auer D, Sartori B, Cvirn G, Mela P, Berensmeier S, Schwaminger SP (2023) Superparamagnetic iron oxide nanoparticles for their application in the human body: Influence of the surface. Heliyon 9(6):e16487

Wang M, Hu D, Yang Y, Shi K, Li J, Liu Q, Li Y, Li R, Pan M, Mo D, Chen W, Li X, Qian Z (2023a) Enhanced chemo-immunotherapy strategy utilizing injectable thermosensitive hydrogel for the treatment of diffuse peritoneal metastasis in advanced colorectal cancer. Adv Sci (Weinh) 10(35):e2303819

Wang W, Zhang G, Wang Y, Ran J, Chen L, Wei Z, Zou H, Cai Y, Han W (2023b) An injectable and thermosensitive hydrogel with nano-aided NIR-II phototherapeutic and chemical effects for periodontal antibacteria and bone regeneration. J Nanobiotechnology 21(1):367

Wu J, Shao Y, Liu J, Chen G, Ho PC (2011) The medicinal use of realgar (As_4S_4) and its recent development as an anticancer agent. J Ethnopharmacol 135(3):595–602

Wu S, Zhu C, Tang D, Dou QP, Shen J, Chen X (2021) The role of ferroptosis in lung cancer. Biomark Res 9(1):82

Xi J, Fang JH, Xiong XM, Gui C, Wang YX, Zhang XQ (2022) Acid water-ground nano-realgar is superior to crude realgar in promoting apoptosis of MCF-7 breast cancer cells. Curr Med Sci 42(4):720–732

Xiao Y, Gu Y, Qin L, Chen L, Chen X, Cui W, Li F, Xiang N, He X (2021) Injectable thermosensitive hydrogel-based drug delivery system for local cancer therapy. Colloids Surf B Biointerfaces 200:111581

Yang FR, Zhao YF, Hu XW, Liu ZK, Yu XD, Li CY, Li XR, Li HJ (2021) Nano-realgar suppresses lung cancer stem cell growth by repressing metabolic reprogramming. Gene 788:145666

Yang R, Chen F, Xu H, Guo Z, Cao C, Zhang H, Zhang C (2022) Exploring the mechanism of realgar against esophageal cancer based on ferroptosis induced by ROS-ASK1-p38 MAPK signaling pathway. Evid Based Complement Alternat Med 2022:3698772

Zhang X, He Z (2023) Cell membrane coated pH-responsive intelligent bionic delivery nanoplatform for active targeting in photothermal therapy. Int J Nanomedicine 18:7729–7744

Zhang S, Cao S, Zhou H, Li L, Hu Q, Mao X, Ji S (2022) Realgar-induced nephrotoxicity via ferroptosis in mice. J Appl Toxicol 42(11):1843–1853

Zhang X, Yang R, Wang H, Cao C, Zhao W, Duan L, Chen F (2024) Inhibition of p62-Keap1-Nrf2 pathway activation by realgar promotes the inhibition of esophageal cancer cell proliferation, migration, and ferroptosis. Curr Drug Deliv 21(2):236–248

Zhou H, Lu X, Du C, Zhou Z, Feng J, Liang Z, Xu Y, Qiu X, Shen Z (2022) Cycloacceleration of reactive oxygen species generation based on exceedingly small magnetic iron oxide nanoparticles for tumor ferroptosis therapy. Small 18(35):e2202705

Publisher's Note